

Marginal Fermi Points and Topological Phase Transitions in Dirac Semimetal $A_3\text{Bi}$ ($A=\text{Na, K, Rb}$)

Zhijun Wang¹, Yan Sun², Xingqiu Chen², Cesare Franchini²,
Gang Xu¹, Hongming Weng^{1,*}, Xi Dai^{1,†} and Zhong Fang^{1‡}

¹*Beijing National Laboratory for Condensed Matter Physics,
and Institute of Physics,
Chinese Academy of Sciences,
Beijing 100190, China;*

and

²*Shenyang National Laboratory for Materials Science, Institute of Metal Research,
Chinese Academy of Sciences, Shenyang 110016, China*

(Dated: February 28, 2012)

Abstract

The vacuum of Standard Model above electroweak transition can be regarded as a system with marginal Fermi points (MFP) [1, 2], which is not stable and may decay into three topologically distinct universality classes, i.e., vacua with gap, fermi surfaces, or Weyl points. We expect that, condensed matters with emerging relativistic quantum field theory in the low energy corner, may be relevant to such physics as well. Here we show, based on first-principles calculations, that crystalline $A_3\text{Bi}$ ($A=\text{Na, K, Rb}$) are three dimensional (3D) Dirac semimetals with MFP protected by crystal symmetry. They possess non-trivial Fermi arcs on the surfaces, and can be driven into various topologically distinct phases by explicit breaking of symmetries. Giant diamagnetism, linear quantum magnetoresistance, and quantum spin-Hall effect will be expected for such novel compounds.

The topological consideration of effective relativistic quantum field theory in 3D momentum space allow us to classify quantum vacua (into three distinct classes) and simulate high-energy physics and cosmology by probing condensed matters [1, 2]. The topological classes with fermi surface or gap are well known in condensed matters as metals or insulators, and the fully gapped systems have been further classified recently into topologically trivial and non-trivial insulators [3–5]. The class of compounds with Weyl fermi points are rare, however, the A-phase of ^3He [6] and recent proposals [7–10] suggested various possibilities. Given those known realizations of distinct topological states, it is still challenging to have a well controlled example near phase boundary such that various topological phase transitions can be studied systematically within one system. This challenge becomes further relevant because the vacuum of Standard Model is regarded to be at the phase boundary with MFP, where two Weyl points with opposite chirality (or topological charge) overlap, forming massless Dirac fermionic gas [1, 2]. The Weyl points with opposite chirality are stable topological objects only if they are separated. If they meet, their topological charges may cancel each other and open a gap. In principle, we may obtain accidental MFP by fine tuning of chemical composition or spin-orbit coupling (SOC) strength [11–14]. Unfortunately, such realizations are too fragile and hard to be controlled. Here we show that, in the presence of crystal symmetry, MFP can be protected and stabilized [15], and this scenario can be achieved in a simple stoichiometry compound $A_3\text{Bi}$ ($A=\text{Na, K, Rb}$), which supports 3D massless gas of Dirac fermions, different with graphene and Weyl semimetals.

Among the alkali pnictides A_3B ($A=\text{Alkali metal, } B=\text{As, Sb or Bi}$), $A_3\text{Sb}$ are well known for its application as photocathode materials [16], but the physical properties of $A_3\text{Bi}$ are not widely studied [17]. Both Li_3Bi and Cs_3Bi crystallize in cubic $Fm\bar{3}m$ structure, while Na_3Bi , K_3Bi and Rb_3Bi are in hexagonal $P6_3/mmc$ phase (or D_{6h}^4 , shown in Fig.1) [18], which are our main focus here by taking Na_3Bi as an example. In this structure [19], there are two nonequivalent Na sites (Na(1) and Na(2)). Na(1) and Bi form simple honeycomb lattice layers which stack along the c -axis, while Na(2) atoms are inserted between the layers, making connection with Bi atoms. From the ionic picture, due to the closed-shell configuration where the number of valence electrons ($3\times\text{Na-}s^1+\text{Bi-}p^3$) is equal to 6, we may expect semiconducting nature of these compounds, similar to Na_3Sb [20]. However, they are in fact different.

The calculated electronic structures (see Methods) shown in Fig. 2 suggest that the

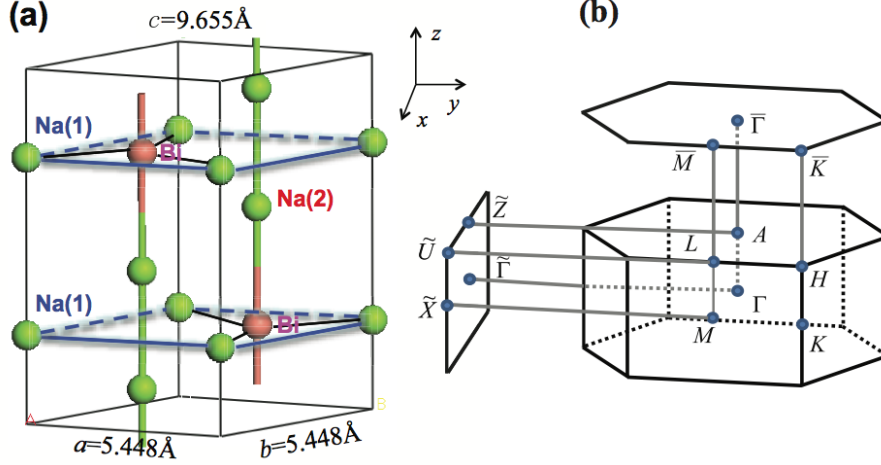


FIG. 1: (Color online) (a) Crystal structure of Na_3Bi with $P6_3/mmc$ symmetry. Na(1) is at $2b$ position $\pm(0,0,\frac{1}{4})$, and Bi is at $2c$ position $\pm(\frac{1}{3},\frac{2}{3},\frac{1}{4})$. They form honeycomb lattice layers. Na(2) are at $4f$ position $\pm(\frac{1}{3},\frac{2}{3},u)$ and $\pm(\frac{2}{3},\frac{1}{3},\frac{1}{2}+u)$ with $u=0.583$, threading Bi along c axis. (b) Brillouin Zone of bulk and the projected surface Brillouin Zones of (001) and (010) plane.

valence and conduction bands are dominated by Bi- $6p$ and Na- $3s$ states. Very close to the Fermi level, the top valence band is mostly from Bi- $6p_{x,y}$ states, while the conduction band with very strong dispersion is mostly from Na(1)- $3s$ states. All these pictures are similar to that of Na_3Sb [20], but with the key difference: at the Γ point, the Na- $3s$ band is lower than Bi- $6p_{x,y}$ by about 0.3eV, and it is further enhanced to be 0.7eV in the presence of SOC, resulting in a metal with inverted band structure, rather than the normal narrow gap semiconductor like Na_3Sb [20]. The band inversion is mostly due to the heavier Bi, which has higher $6p$ -states and larger SOC compared to Sb. Considering the possible underestimation of band gap by GGA, the band inversion can be further confirmed by the following evidences: (1) calculation using hybrid functional (HSE) [21] gives band inversion around 0.5 eV, still reasonably strong; (2) the earlier calculations for normal semiconductor K_3Sb [22] suggest that its experimental gap can be reasonably reproduced by LDA.

Having the inverted band structure, however, Na_3Bi is not gapped, different from topological insulators like Bi_2Te_3 and Bi_2Se_3 [23]. It is a semi-metal with two nodes (band-crossings) exactly at fermi level (Fig.2). In other words, its fermi surface consists of two isolated fermi points, which are located at $(0, 0, k_z^c \approx \pm 0.26 \times \frac{\pi}{c})$ along the Γ -A line. Since both time reversal and inversion symmetries are present, there are four-fold degeneracy at each fermi

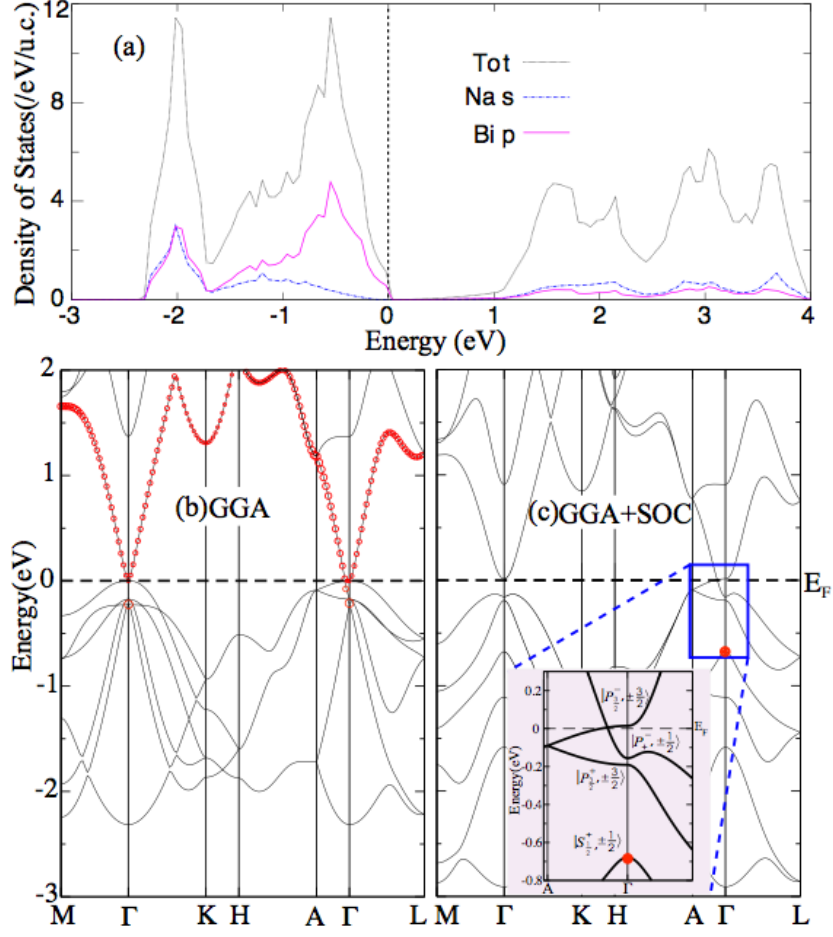


FIG. 2: (Color online) The calculated electronic structures of Na_3Bi . (a) The total and partial density of states. (b) and (c) are the band structures without and with spin-orbit coupling, respectively. The red circles indicate the projection to the Na-3s states. The orbital characters of wave-functions at Γ point are labeled in the inset (see Method for details).

point, around which the band dispersions can be linearized, resulting in a 3D massless Dirac semimetal. It is different from graphene not only in dimensionality, but also in its robustness, because the fermi points here survive in the presence of SOC. This fact also makes difference with other proposals [24, 25].

The 4×4 Dirac fermion here is massless because the two bands which cross each other along the Γ -A line belong to different irreducible representations under three-fold rotational symmetry. Breaking of this symmetry will make the system insulating. For example, 1% compression along y will open up a gap $\approx 5.6\text{meV}$. This insulating state, however, is topologically non-trivial with $Z_2=1$ [3, 4] due to the inverted band structure around the Γ point.

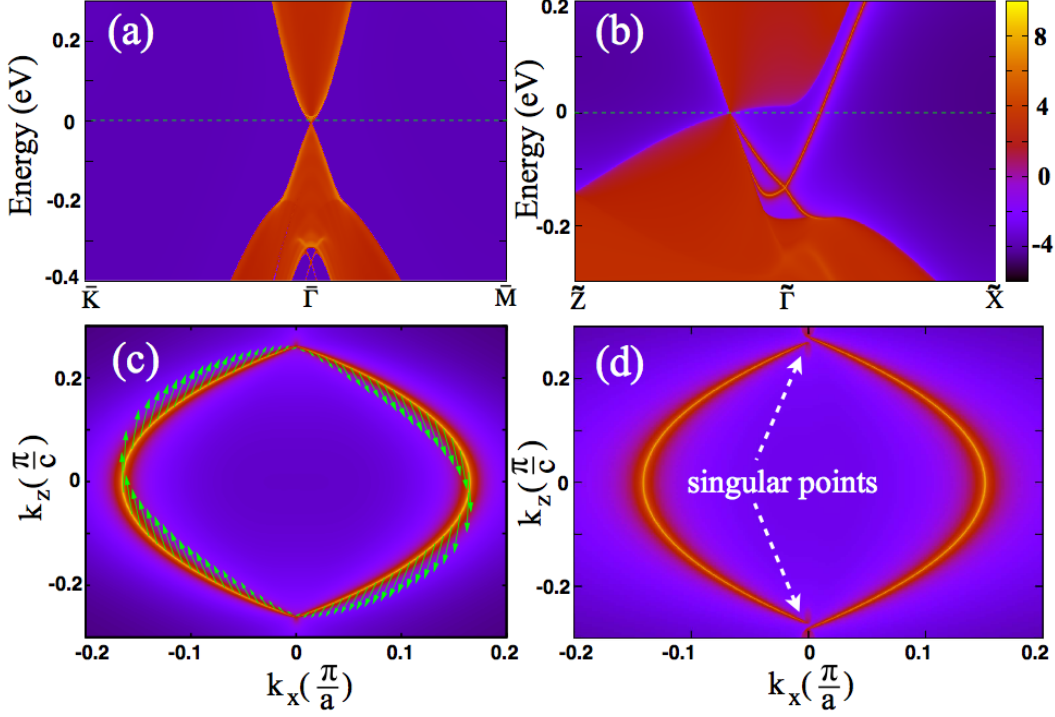


FIG. 3: (Color online) The projected surface states and their Fermi surfaces of Na_3Bi . (a) and (b) are the surface states for (001) and (010) surfaces, respectively. (c) The Fermi surfaces (Fermi arcs) and its spin texture (in-plane component) for the (010) surface states. (d) The Fermi arcs of (010) surface obtained from fitted effective Hamiltonian with additional exchange field $h_1=6$ meV (see Method for details). The discontinuity around the singular Fermi points becomes now obvious.

This fact makes Na_3Bi unique, because both bulk Fermi points and non-trivial surface states (a single pair) should coexist (see Fig. 3) as long as the crystal symmetry stands. Furthermore, the surface states are different from that of topological insulators [23], in the sense that its Fermi surface has Fermi arc structures. As shown in Fig. 3(b) for the (010) surface of stoichiometry Na_3Bi , although the entire Fermi surface is closed, its derivative and Fermi velocity are ill defined at the two singular points (corresponding to the projection of bulk Fermi points to the surface). The spin texture of surface states has a helical structure (also similar to topological insulators), but the magnitude of spin vanishes at the singular points. This kind of Fermi surfaces has never been found before, and it can be understood following the discussions for Weyl semimetal [7, 8]. If we split the 4×4 Dirac point into two separated 2×2 Weyl points in momentum space by breaking time reversal or inversion symmetry [9, 10], the Fermi surface of surface states will also split into open segments which are Fermi arcs

discussed in Weyl semimetal (as shown in Fig.3d) [7, 8]. All these characters in contrast to conventional metals and topological insulators should be experimentally measurable by nowadays ARPES technique. Our further calculations for K_3Bi and Rb_3Bi suggest that they have qualitatively the same pictures as Na_3Bi .

Effective Hamiltonian

The low energy physics here can be understood from effective Hamiltonian. At the Γ point, the low energy eigen states can be approximated as the linear combination of Na-3s and Bi-6p atomic orbitals. Among them, we focus on the four states $|S_{\frac{1}{2}}^+, +\frac{1}{2}\rangle$, $|P_{\frac{3}{2}}^-, +\frac{3}{2}\rangle$, $|S_{\frac{1}{2}}^+, -\frac{1}{2}\rangle$, $|P_{\frac{3}{2}}^-, -\frac{3}{2}\rangle$, which capture the band inversion nature (see methods, here the superscript \pm indicate the parity of each state). We can then construct an effective 4×4 $k \cdot p$ Hamiltonian using these four states as basis. Considering the time reversal, inversion, and D_{6h}^4 symmetries, the leading order Hamiltonian around Γ reads:

$$H_{\Gamma}(\mathbf{k}) = \epsilon_0(\mathbf{k}) + \begin{pmatrix} M(\mathbf{k}) & Ak_+ & 0 & B^*(\mathbf{k}) \\ Ak_- & -M(\mathbf{k}) & B^*(\mathbf{k}) & 0 \\ 0 & B(\mathbf{k}) & M(\mathbf{k}) & -Ak_- \\ B(\mathbf{k}) & 0 & -Ak_+ & -M(\mathbf{k}) \end{pmatrix}$$

where $\epsilon_0(\mathbf{k}) = C_0 + C_1k_z^2 + C_2(k_x^2 + k_y^2)$, $k_{\pm} = k_x \pm ik_y$, $B(\mathbf{k}) = B_3k_zk_+^2$, and $M(\mathbf{k}) = M_0 - M_1k_z^2 - M_2(k_x^2 + k_y^2)$ with parameters $M_0, M_1, M_2 < 0$ to ensure band inversion. Please note the leading order term of off-diagonal elements $B(\mathbf{k})$ has to take the form of $k_zk_+^2$ under three fold-rotational symmetry and the opposite parity of $|S\rangle$ and $|P\rangle$ states. Evaluating the eigen values $E(\mathbf{k}) = \epsilon_0(\mathbf{k}) \pm \sqrt{M(\mathbf{k})^2 + A^2k_+k_- + |B(\mathbf{k})|^2}$, we get two gapless solutions at $\mathbf{k}^c = (0, 0, k_z^c = \pm\sqrt{\frac{M_0}{M_1}})$, which are the MFP discussed above. There is a pair of such points, which are separated along the $\Gamma - A$ line.

If we only concentrate to the neighborhood of each crossing points \mathbf{k}^c , and neglect the high order terms (i.e., $B(\mathbf{k}) \approx 0$), the linearized Hamiltonian is nothing but 3D massless Dirac fermions. The block diagonal form allows us to decouple the 4×4 matrix into two 2×2 matrices, which are Weyl fermions with degenerate energy but opposite chirality [7–10]. The violation of three-fold rotational symmetry, however, will introduce a linear leading order term of $B(\mathbf{k})$, i.e., $B(\mathbf{k}) = B_1k_z$. In such case, two Weyl fermions will be coupled together, resulting in massive Dirac fermions with gap, similar to the case of Bi_2Se_3 or Bi_2Te_3 [23, 26].

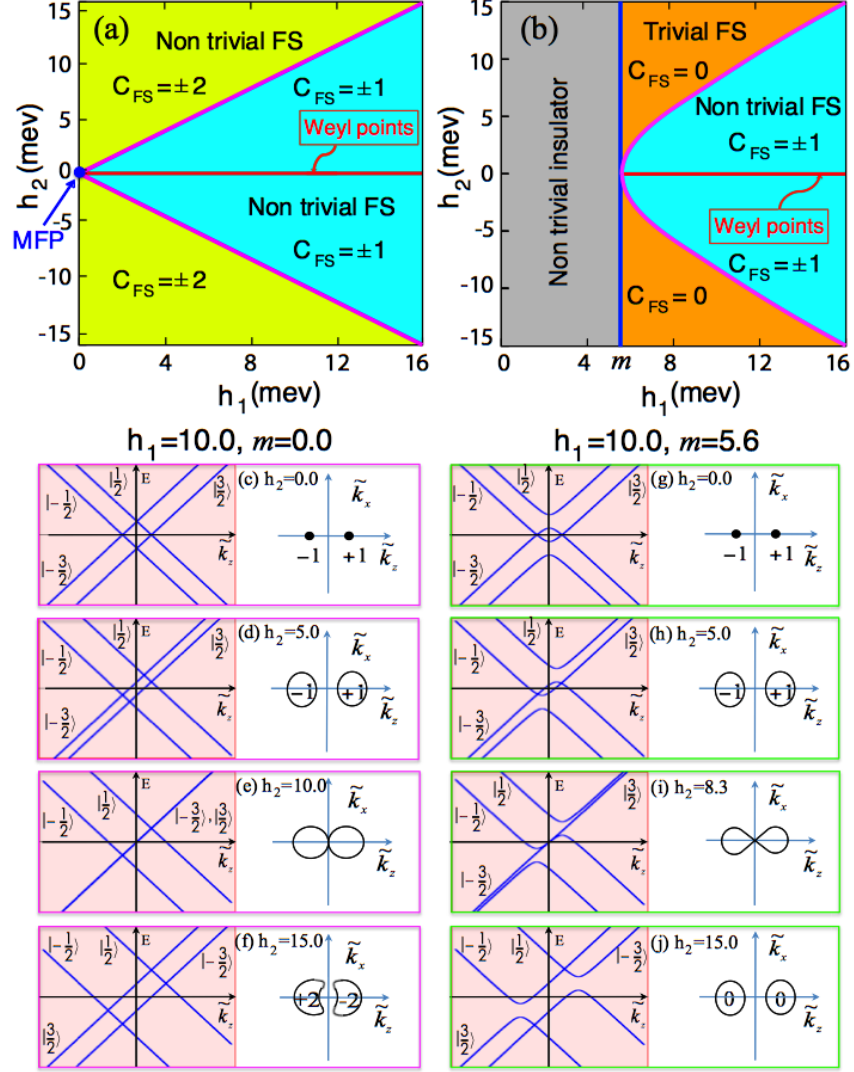


FIG. 4: (Color online) Phase diagrams of Na_3Bi with mass term $m=0$ (left panels) and $m=5.6\text{meV}$ (right panels). The high order term of $B(\mathbf{k})$ is neglected for the case of $m=5.6\text{meV}$. (a) and (b) are phase diagrams, and (c)-(j) show band dispersions, corresponding fermi surfaces and its topological charges for some characteristic phases (with h_1 fixed to be 10.0 meV). Only the neighborhood around one of the MFP is show with the $\tilde{\mathbf{k}}$ defined as $\mathbf{k} - \mathbf{k}^c$. The $|\pm \frac{1}{2}\rangle$, $|\pm \frac{3}{2}\rangle$ are abbreviations (i.e. J_z values) for the four basis, which are used to indicate the main component of the wavefunctions for the states away from band crossings. (see text part for details).

Nevertheless, as long as the three-fold rotational symmetry survives, the MFP here should be stable and protected.

Phase diagram and topological phase transitions

Na_3Bi with MFP is just located at phase boundary and may be driven into various topologically distinct states by explicit breaking of symmetries [1, 2]. For simplicity of illustration, here we focus on the effects of exchange splitting, assuming it can be induced by magnetic doping. Other symmetry-breaking terms (such as inversion, mirror or two fold rotational symmetries of the crystal) may play the same roles and can be analyzed analogously. Since the $|S\rangle$ and $|P\rangle$ are different orbitals (or pseudo spins), we may in general separate any exchange splitting into orbital dependent and independent parts as $H_{ex1} = h_1 \sigma_z \otimes \tau_z$ and $H_{ex2} = h_2 \sigma_z \otimes I$, where h_1 and h_2 are field strength (along z direction), and $\vec{\sigma}$ and $\vec{\tau}$ are pauli matrices describing spin and pseudo-spin respectively. The total Hamiltonian is given as $H = H_\Gamma + H_{ex1} + H_{ex2}$, and the resulting phase diagram is shown in Fig.4.

If the three fold rotational symmetry of crystal is preserved (i.e. $B(\mathbf{k}) = B_3 k_z^c k_+^2$, left panels of Fig.4), starting from the MFP state ($h_1=0, h_2=0$), the state with Weyl points will be introduced by h_1 (horizontal axis), because such exchange field will split the Dirac point into two separated Weyl points in momentum space. If the h_2 is further introduced, however, the two Weyl points will separate energetically, and a system with fermi surfaces (FS) will be obtained. On the other hand, if the three-fold rotational symmetry is broken, a mass term $m \approx B_1 k_z^c$ will be induced, and the high order term of $B(\mathbf{k})$ can be then neglected. In such case, a topologically non-trivial insulating phase will appear (right panels of Fig.4), and the Weyl semimetal phase can be driven only if h_1 is larger than the mass term m .

The FS states can be further classified according to their enclosed topological charge (or Chern number C_{FS}), which is defined as the net flux of the Berry phase gauge field penetrating the fermi surface,

$$C_{FS} = \frac{1}{2\pi} \int_{FS} (\nabla_{\mathbf{k}} \times \mathbf{A}(\mathbf{k})) \cdot d\mathbf{S}$$

where the integrand is the Berry curvature, $\mathbf{A}(\mathbf{k}) = -i\langle u_{\mathbf{k}} | \nabla_{\mathbf{k}} | u_{\mathbf{k}} \rangle$ is the adiabatic Berry connection for the states $|u_{\mathbf{k}}\rangle$ at fermi level, and $d\mathbf{S}$ points from low to high energy. For the case $m=5.6\text{meV}$ (right panels), the two distinct FS states, trivial ($C_{FS} = 0$) and non-trivial ($C_{FS} = \pm 1$), are separated by the line defined as $h_1^2 - h_2^2 = m^2$. If $m = 0$ (left panels), both FS states are non-trivial, but with different topological charges ($C_{FS} = \pm 1$ or ± 2). The appearance of $C_{FS} = \pm 2$ phase in this case is due to the $B_3 k_z k_+^2$ term of $B(\mathbf{k})$. At the

boundary between distinct FS states, the fermi spheres should be connected, and the C_{FS} becomes ill-defined. The non-trivial FS states may become important for the topological superconductivity [27].

Even without the exchange splitting, we can expect somethings particular for such novel compounds. First of all, we will expect quantum spin Hall effect in z -oriented Na_3Bi thin film (or $\text{Na}_3\text{Bi}/\text{Na}_3\text{Sb}$ quantum well). Due to the quantum size effect, the k_z is further quantized, and in general the 2D band structures of Na_3Bi thin film will be fully gapped. Then depending on the number of band inversions associated with the subbands, the system should crossover between trivial and non-trivial 2D insulators oscillatorily as a function of film thickness [28]. Our estimated first critical thickness of Na_3Bi is 35\AA , below (above) which the film is a trivial (non-trivial) insulator. Secondly, we will expect giant diamagnetism of 3D massless Dirac fermion [29]. The diamagnetic susceptibility, $\chi(\varepsilon) \sim \log \frac{1}{\varepsilon}$, should diverge logarithmically when the chemical potential approaches the MFP (i.e. $\varepsilon \sim 0$) [29], much stronger than that in narrow gap semimetals like Bismuth. Thirdly, we will also expect linear quantum magnetoresistance (MR) as proposed by A. A. Abrikosov [30]. In conventional metals with closed fermi surface, the MR should behavior quadratically at low field and saturate at high field. However, for the 3D massless Dirac fermionic gas, the MR will have linear field dependence if only the lowest Landau level is occupied. This idea have been examined for the Ag_2Te both experimentally and theoretically [30, 31], where the Dirac type energy dispersion is not obvious. Having Na_3Bi with MFP, it will be straightforward to check the quantum MR proposal [30]. Finally, it will be very interesting to study the possible simultaneous symmetry-breaking introduced by interactions.

We acknowledge the supports from NSF of China, the 973 program of China, and the Hundred Talents Project of the Chinese Academy of Sciences.

METHODS

First-principles calculations are preformed based on the plane-wave ultra-soft pseudopotential method, using the generalized gradient approximation (GGA) for the exchange-correlation functional. The calculations based on hybrid functional (HSE) [21] are further supplemented to check the band gap. The cutoff energy for wave-function expansion is 25 Ry, and the k-point sampling is $12 \times 12 \times 6$. The experimental lattice parameters [19] are

used, and the calculations are well converged with respect to above settings. The projected surface states are obtained from the surface Green's function of semi-infinite system, similar to the method used for Bi₂Te₃ and Bi₂Se₃ [12, 23]. For this purpose, we construct the maximally localized Wannier functions (MLWF) from the first-principles calculations.

The low energy effective hamiltonian is derived from the theory of invariants in a similar way as that for Bi₂Se₃, Bi₂Te₃ and Sb₂Te₃ [26]. The first-principles calculations indicate that the wave-functions of low energy states at Γ point are mostly from the Na-3s and Bi-6 $p_{x,y,z}$ orbitals. For the low energy Na-3s at Γ , about 65% characters are from Na(1)-3s and 35% from Na(2)-3s. Since the system has inversion symmetry, the wave-functions at Γ point have definite parity. There are two formula units in each unit cell, and they form bonding and anti-bonding configurations. Finally the linear combination of atomic orbitals read:

$$|S^\pm\rangle = \frac{1}{\sqrt{2}}(|Na, s\rangle \pm |Na', s\rangle),$$

$$|P_\alpha^\pm\rangle = \frac{1}{\sqrt{2}}(|Bi, p_\alpha\rangle \mp |Bi', p_\alpha\rangle),$$

where Na(Bi) and Na'(Bi') are related by inversion symmetry. The superscript \pm indicates the parity, and α is p_x , p_y or p_z .

Taking $|S^\pm\rangle$ and $|P_\alpha^\pm\rangle$ as new atomic orbitals, and including SOC effect, spin and orbital angular momenta will be coupled, and the standard eigenstates can be written as $|S_{\frac{1}{2}}^\pm, \pm\frac{1}{2}\rangle$, $|P_{\frac{3}{2}}^\pm, \pm\frac{3}{2}\rangle$, $|P_{\frac{3}{2}}^\pm, \pm\frac{1}{2}\rangle$, $|P_{\frac{1}{2}}^\pm, \pm\frac{1}{2}\rangle$, where the subscript indicates the total angular momentum J . Different from the case with Zinc-blende structure (such as HgTe), here the heavy-hole state $|P_{\frac{3}{2}}^\pm, \pm\frac{3}{2}\rangle$ and light-hole states $|P_{\frac{3}{2}}^\pm, \pm\frac{1}{2}\rangle$ are no longer degenerated at Γ point, because Bi atoms are sandwiched by Na(2) atoms along z -axis, and Bi p_z orbital is lower than $p_{x,y}$ orbitals. Furthermore, under the D_{6h}^4 symmetry, the light-hole state $|P_{\frac{3}{2}}^\pm, \pm\frac{1}{2}\rangle$ and split-off state $|P_{\frac{1}{2}}^\pm, \pm\frac{1}{2}\rangle$ will mix further to form the new eigen states: $|P_+^\pm, \pm\frac{1}{2}\rangle$ and $|P_-^\pm, \pm\frac{1}{2}\rangle$ [26]. Nevertheless these mixed states are not relevant to our discussions for the MFP. The band inversion and their crossings along Γ -A line can be described by four states $|S_{\frac{1}{2}}^+, \pm\frac{1}{2}\rangle$ and $|P_{\frac{3}{2}}^-, \pm\frac{3}{2}\rangle$. Different from Bi₂Se₃ [26], where all the four basis have the same $|J_z|=\frac{1}{2}$, here they have two different values of $\frac{1}{2}$ and $\frac{3}{2}$, respectively. This difference is essential to the existence and stability of 3D Dirac points observed here.

The parameters in the effective hamiltonian are fitted to the first-principles band structures. Their values are: $C_0=-0.06382$ eV, $C_1=8.7536$ eVÅ², $C_2=-8.4008$ eVÅ², $M_0=-0.08686$ eV, $M_1=-10.6424$ eVÅ², $M_2=-10.3610$ eVÅ², $A=2.4598$ eVÅ.

-
- * Electronic address: hmweng@aphy.iphy.ac.cn
- † Electronic address: daix@aphy.iphy.ac.cn
- ‡ Electronic address: zfang@aphy.iphy.ac.cn
- [1] Klinkhamer, F. R. & Volovik, G. E. Emergent CPT violation from the splitting of Fermi points Int. J. Mod. Phys. A **20**, 2795 (2005).
 - [2] Volovik, G. E. *The Universe in a Helium Droplet* (Clarendon Press, Oxford), 2003.
 - [3] Hasan, M. Z. & Kane, C. L. Colloquium: Topological insulators. Rev. Mod. Phys. **82**, 3045 (2010).
 - [4] Qi, X.-L. & Zhang, S.-C. Topological insulators and superconductors. Rev. Mod. Phys. **83**, 1057 (2011).
 - [5] Schnyder, A. P. et al. Classification of topological insulators and superconductors in three spatial dimensions. Phys. Rev. B **78**, 195125 (2008).
 - [6] Leggett, A. J. A theoretical description of the new phases of liquid ^3He . Rev. Mod. Phys. **47**, 331 (1975).
 - [7] Wan, X.-G., Turner, A. M., Vishwanath, A. & Savrasov, S. Y. Topological semimetal and Fermi-arc surface states in the electronic structure of pyrochlore iridates. Phys. Rev. B **83**, 205101 (2011).
 - [8] Xu, G., Weng H.-M., Wang, Z.-J., Dai, X. & Fang, Z. Chern Semimetal and the Quantized Anomalous Hall Effect in HgCr_2Se_4 . Phys. Rev. Lett. **107**, 186806 (2011).
 - [9] Burkov, A. A. & Balents, L. Weyl Semimetal in a Topological Insulator Multilayer. Phys. Rev. Lett. **107**, 127205 (2011).
 - [10] Burkov, A. A., Hook, M. D. & Balents, L. Topological nodal semimetals. Phys. Rev. B **84**, 235126 (2011).
 - [11] Murakami, S. Phase transition between the quantum spin Hall and insulator phases in 3D: emergence of a topological gapless phase. New J. Phys. **9**, 356 (2007).
 - [12] Zhang, W., Yu, R., Zhang, H.-J., Dai, X. & Fang, Z. First-principles studies of the three dimensional strong topological insulators Bi_2Te_3 , Bi_2Se_3 and Sb_2Te_3 . New J. Phys. **12**, 065013 (2010).
 - [13] Xu, S. Y. et al. Topological phase transition and texture inversion in a tunable topological

- insulator. *Science* **332**, 560 (2011).
- [14] Sato, T. et al. Unexpected mass acquisition of dirac fermions at the quantum phase transition of a topological insulator. *Nature Phys.* **7**, 840 (2011).
 - [15] Young, S. M., Zaheer, S., Teo, J. C. Y., Kane, C. L., Mele, E. J. & Rappe, A. M. Dirac semimetal in three dimensions. arXiv:1111.6483 (2011).
 - [16] Wei, S. H. & Zunger, A. Electronic structure of $M_3^I Sb$ -type filled tetrahedral semiconductors. *Phys. Rev. B* **35**, 3952 (1987).
 - [17] Tegze, M. & Hafner, J. Electronic structure of alkali-pnictide compounds. *J. Phys.: Cond. Matt.* **4**, 2449 (1992).
 - [18] Massalski, T. B. *Binary Alloy Phase Diagrams*, (ASM International, Materials Park, Ohio), 1990.
 - [19] Brauer, G. & Zintl, E. Z. Metals and Alloys.23. Constitution of Phosphides, Arsenides, Antimonides and Bismuthides of Li, Na and K. *Phys. Chem., Abt. B* **37**, 323 (1937).
 - [20] Ettema, A. R. H. F. & de Groot, R. A. Electronic structure of Na₃Sb and Na₂KSb. *Phys. Rev. B* **61**, 10035 (2000).
 - [21] Heyd, J., Scuseria, G. E. & Ernzerhof, M. Erratum: " Hybrid functionals based on a screened Coulomb potential" [*J. Chem. Phys.* 118,8207 (2003)]. *J. Chem. Phys.* **124**, 219906 (2006).
 - [22] Ettema, A. R. H. F. & de Groot, R. A. Band structure calculations of the hexagonal and cubic phases of K₃Sb. *J. Phys.: Cond. Matt.* **11**, 759 (1999).
 - [23] Zhang H.-J. et al. Topological insulators in Bi₂Se₃, Bi₂Te₃ and Sb₂Te₃ with a single Dirac cone on the surface. *Nature Phys.* **5**, 438 (2009).
 - [24] Kino, H. & Miyazaki, T. First principles study of electronic structure in α -(BEDT-TTF)₂I₃ at ambient pressure and with uniaxial strain. *J. Phys. Soc. Jpn.* **75**, 034704 (2006).
 - [25] Pardo, V. & Pickett, W. E. Half-metallic semi dirac point generated by quantum confinement in TiO₂/VO₂ nanostructures. *Phys. Rev. Lett.* **102**, 166803 (2009).
 - [26] Liu C.-X., Qi, X.-L., Zhang, H.-J., Dai, X., Fang, Z. & Zhang, S. C. Model Hamiltonian for topological insulators. *Phys. Rev. B* **82**, 045122 (2010).
 - [27] Qi, X. L., Hughes, T. L. & Zhang, S. C. Topological invariants for the fermi surface of a time-reversal-invariant superconductor. *Phys. Rev. B* **81**, 134508 (2010).
 - [28] Liu, C.-X. et al. Oscillatory crossover from two-dimensional to three-dimensional topological insulators. *Phys. Rev. B* **81**, 041307 (2010).

- [29] Koshino, M. & Ando, T. Anomalous orbital magnetism in dirac electron system: role of pseudospin paramagnetism. Phys. Rev. B **81**, 195431 (2010); and see references therein.
- [30] Abrikosov, A. A. Quantum magnetoresistance. Phys. Rev. B **58**, 2788 (1998); and see references therein.
- [31] Zhang, W., Yu, R., Feng W., Yao, Y., Weng, H. M., Dai, X. & Fang, Z. Topological Aspect and Quantum Magnetoresistance of $\beta - Ag_2Te$. Phys. Rev. Lett. **106**, 156808 (2011).